Available online at www.sciencedirect.com
ScienceDirect
Journal of Sound and Vibration 302 (2007) 425–441
JOURNAL OF SOUND AND VIBRATION
www.elsevier.com/locate/jsvi

Forced vibrations of two nonlinearly connected solid waveguides under static load

I.K. Vagapov*, M.M. Ganiev, A.S. Shinkarev

Kazan State Technical University "A. N. Tupolev" 420111, Karl Marx street, 10, Kazan, Republic of Tatarstan, Russian Federation

Received 24 June 2002; received in revised form 25 August 2005; accepted 1 February 2006
Available online 9 February 2007

Abstract

Forced impact oscillations in nonlinearly coupled solid waveguides with nearly equal natural frequencies are examined using the harmonic balance method. A dynamic model is used to describe the process of ultrasonic micro-forging where the material to be worked is considered as a nonlinear connecting-link between the ultrasonic transducer and passive waveguide-reflector. The influence of the material properties (yield stress, stiffness of tool–workpiece contact, striker and blank geometries) and the processing conditions (amplitude of vibration, static compressive force, work rate) on the resonance characteristics of the vibratory system is taken into account. The resonance and antiresonance frequencies, boundaries of response stability, ranges of inphase and antiphase oscillations of impacting waveguides, and some other features of strongly coupled vibrators under impact loading are determined.

It is shown also that the largest amplitude of impact oscillations can be attained only if the natural frequency of the ultrasonic transducer exceeds that of the waveguide-reflector. By measuring the dynamic drift in the unfastened ultrasonic unit, it is possible to control, directly in the course of ultrasonic micro-forging, the thickness of the metal workpiece. Calculated data are compared with the experimental results.

1. Introduction

In ultrasonics, wide use is made of vibratory systems where a workpiece is placed between the end faces of longitudinal vibration-type waveguides pressed in contact with each other [1–4]. One of these waveguides (or both) is excited by a high-power electromechanical transducer. The workpiece is subjected to repeated impacts. A compressive force is applied to the supporting flanges at the waveguide nodal planes, and the workpiece is placed at the displacement maximum of the longitudinal standing wave. The dynamics of ultrasonic machining may be considered as the forced vibrations of two resonant subsystems coupled via the workpiece; the latter acts both as the processing load and the connecting link.

A distinguishing feature of ultrasonic machining is the high-frequency vibro-impact interaction between the tool and the blank that results in small but cumulative residual plastic strains during every load cycle [5,6]. The

*Corresponding author. Vosstanyia street, 49-30 Kazan, 420080, Republic of Tatarstan, Russian Federation. Tel.: +7 8432 450393; fax: +7 8432 987023.
E-mail address: rustemiv@yandex.ru (I.K. Vagapov).

0022-460X/$ - see front matter © 2006 Elsevier Ltd. All rights reserved.
doi:10.1016/j.jsv.2006.02.002

order of magnitude of the impact duration is comparable with that of the ultrasound period; so the impact cannot be considered instantaneous.

In order to ensure resonance excitation in both waveguides at the same frequency, the difference between their natural frequencies must be chosen to be less than the bandwidth of the resonance peak in the unloaded waveguide; otherwise, the use of an additional resonant waveguide is meaningless. In practice, the natural frequencies of real engineering waveguides differ slightly in magnitude due to manufacturing inaccuracy, distinctions in acoustic properties, non-identity and wear of machining tools attached to these waveguides [2].

A shortcoming of ultrasonic devices equipped with only one resonant vibrator is that the massive non-resonant support (anvil) used to support a blank against the waveguide's end face acts at the same time as a vibration damper. In cases where a thin specimen is clamped between two waveguides tuned to resonate at the same frequency, a longitudinal standing wave can be excited in the coupled vibrating system as a whole, while the mounting flanges (used for fixing the waveguides) can be placed precisely at the standing wave nodes. Owing to the elimination of wave leakages into the non-resonant supporting frame of the machine, this scheme makes it possible to optimize vibration isolation and energy conservation in the system; in addition, it allows redoubling of input power supplied [3]. The advantages of the scheme considered here are of great significance when machining brittle, hard, and high-strength materials (where a need exists for high-power vibrations in the presence of the maximum admissible force of static compression [2,5–7]).

On the other hand, introduction of the additional resonator results in the appearance of two neighboring eigenfrequencies that correspond to the inphase and antiphase oscillation in the coupled vibrators [8]. It should be noted that the inphase oscillation gives rise to motion of adjacent end faces of waveguides towards each other; for this reason, it is this vibration mode that is solely suitable for material machining in the impact regime [9]. The connecting-link between these two ultrasonic waveguides must be thus considered as a nonlinear (impacting) and dissipative link. The coupling strength depends on the mechanical properties of the material worked and a number of technological factors (largely, on the compression force value) [10]. Any variations of the load, and the nonlinear nature of interaction between the tool and the blank, make it difficult to sustain the resonance of impact oscillation while tuning out the useless antiphase mode that corresponds to the end faces moving in the same direction [9]. A similar problem associated with tuned frequency isolation from nearby modes has been considered for multiple-blade ultrasonic cutting devices [11].

The basic features of linear vibrating systems with two degrees of freedom are expounded in Ref. [8]. The system of two identical linearly coupled oscillators is considered in Ref. [12], where the authors predict the existence of symmetric, anti-symmetric and chaotic modes. Mutual influence of two oscillators with nearly equal natural frequencies is examined in Ref. [13]. Also shown here is the fact that, in the presence of a definite ratio of values of natural frequencies, bandwidth and coefficient of coupling, one of the two resonance peaks disappears. In Ref. [14] Cveticanin established the fact that the motion of two-mass system with nonlinear connection can be treated as a combination of translational and oscillatory motions. The period of oscillation depends in this case on the factor of nonlinearity and vibrational amplitude. The influence of coupling strength and frequency of excitation upon the periodic and chaotic motion of a forced impact oscillator that is coupled linearly with a second harmonic oscillator is investigated in Ref. [15]. Theoretical investigation to reduce undesirable nonlinearities of an ultrasonic system has been carried out in the context of 'Nonlinear Cancellation Coupling' of two degree of freedom systems [16]. Application of this method to the high power ultrasonic cutting assembly, consisting of the transducer and half-wavelength blade, proved capable of reducing the effect of the nonlinearities within the vibratory system.

Despite their similarity to the present ultrasonic vibro-impact system, all these systems from Refs. [12–16] must be regarded as linear or nonlinear cases of non-dissipative inseparable coupling, since the interruption of a contact between the vibrators never takes place in reality.

Nonlinear models of tool–workpiece contact interaction accounting for machining processes with superimposed ultrasonic vibration are developed in Refs. [4–6,17,18]. On the assumption that the contact interaction force is a sum of elasto-plastic and dry friction components, the vibro-impact and permanent contact regimes of ultrasonic cutting have been investigated [5]. The influence of static load on ultrasonic percussive drilling is explained using nonlinear models based on the concept of pure impact and impact with dry friction [6]. A relief of plastic flow due to reduction of friction forces in metal forming processes with the use of radially oscillating die [17] and upsetting of specimen between two parallel rigid dies [4] are considered.

The dynamics of an impact oscillator with drift is investigated by means of the intermittent contact interaction model [18]. Each period of oscillation is divided into four intervals corresponding to distinct phases of contact interaction, and is described by four piecewise linear differential equations.

The longitudinal impact oscillations of two identical viscoelastic rods are studied in Refs. [9,19] assuming same problem with absolute rigidity of the contacting end faces the non-identical waveguides is studied in Ref. [2]. Also studied are some variations in the amplitude–frequency characteristic (AFC) and phase-frequency characteristic (PFC), regions of unstable oscillation, appearance of inphase and antiphase eigenmodes and some other dynamic peculiarities.

In the present paper, analysis is made of the forced impact vibration of two non-identical coupled waveguides by using the model for impact deformation [10] that is used conventionally for cold deformation of metals (forging, flatting, and pressing). As distinct from the approximation of infinitely rigid contact [19], this approach makes it possible to derive the relations that describe the interdependence between the technological parameters and resonance characteristics (responses) of the vibratory system. The calculated data are compared here with those obtained experimentally during ultrasonic micro-forging, and are used to develop a new technology for sharpening blades of surgical instruments [7].

2. Dynamic model of ultrasonic micro-forging

Fig. 1 shows the layout of the machining system, consisting of two coaxial waveguides designed as stepped half-wavelength horns. A working tool (striker) either is fastened to the horn's end face or is designed to be integral with the horn (Fig. 1(a)). An ultrasonic transducer can be connected to the rear end of the horn through a tightening screw. One of the waveguides (lower) is fixed rigidly at the node of vibration, while the other one (upper) can move along the longitudinal axis, with its working end face (or striker) pressed to that of the fixed waveguide. An edge of flat blank is drawn continuously through the gap between the waveguides at a

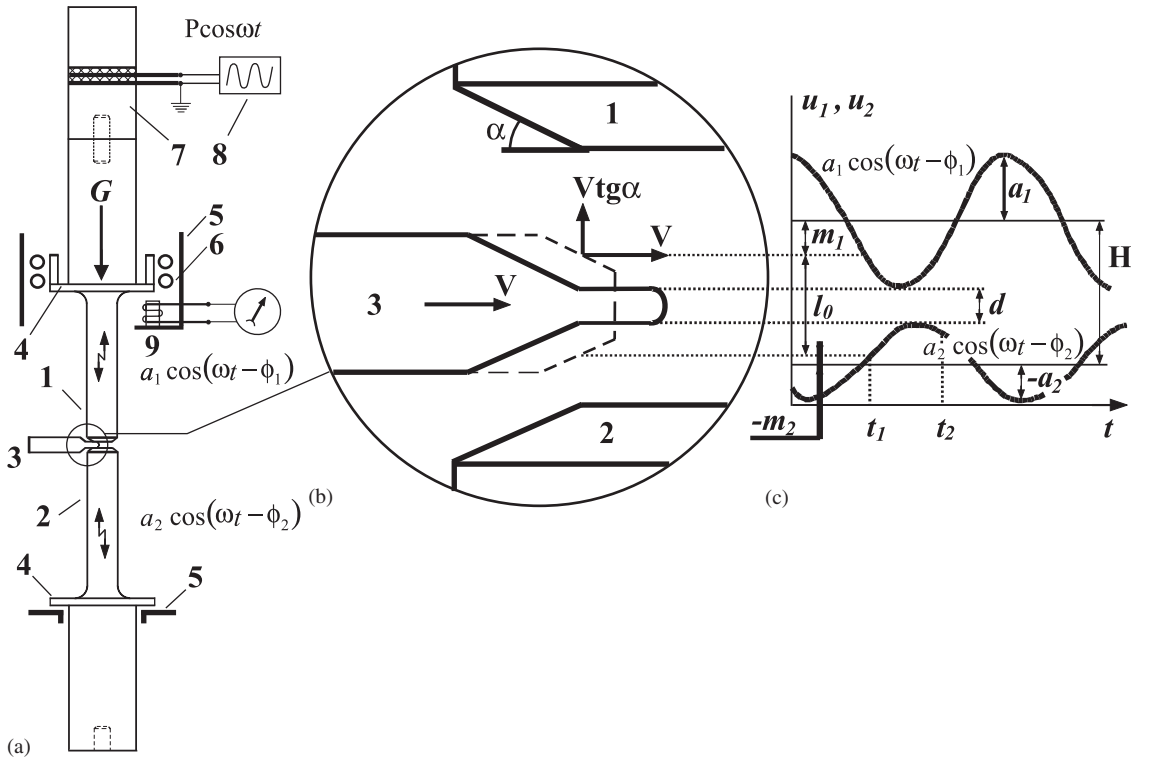

Fig. 1. (a) Scheme of ultrasonic micro-forging set up, 1—forced (active) waveguide, 2—passive waveguide-reflector, 3—blank, 4—flange, 5—framework, 6—linear ball-bearing, 7—transducer, 8—electronic generator, 9—linear motion gauge; (b) scheme of deformation site; dashed line shows the blank's cross-section shape before the collision; (c) time history of strikers vibration.

constant speed. The static force G is applied to a flange situated at the node of vibration of movable ultrasonic unit 1.

When the workpiece is absent and the ultrasonic transducer is de-energized, the strikers' tops are brought into a contact with each other, the gap between strikers is closed, and the upper movable unit 1 is in its lower position. With the ultrasonic generator switched-on and the blank edge fed into the site of deformation, the upper unit has a mean displacement H measured with the use of the gauge 9. In the nonlinear or impact vibrating systems, the occurrence of constant time-independent component or slow drift, in parallel with fast vibration, is a well-known phenomenon [4,6,12,13]. The value of H depends on a number of dynamic characteristics (applied power, amplitudes, phases, damping, etc) and processing conditions (pressing force, speed of the material feed, mechanical properties of work material, blank thickness, geometry of strikers, etc.); it is clear that during the steady-state stationary regime of machining, the dynamic drift value H remains unchanged.

The forging regime of operation (i.e., impact working) can be realized only if the amplitude of velocity of the strikers' relative vibration exceeds the projection of feed velocity onto the direction of longitudinal vibration: $a_V\omega > 2V\tan\alpha$, where V is the component of feed velocity that is directed to the center of the round-shaped striker, and α is the angle of the striker's conical surface inclination. When passing through the site of deformation, the blank is subjected to a large number of impacts; as a result, the blade's cutting edge is formed gradually into a tapered wedge with a small flat burr on its top. The so-attained decrease in the edge thickness, d, specifies a degree of sharpness in the blade made [7]. The presence of complex pattern of metal yield in the site of deformation makes the rigorous calculation of deforming force difficult; for this reason, it is necessary to approximate the waveguides interaction through the work piece using the simple analytical expressions (see the below-given Eqs. (4) and (5)).

Let us consider now the ultrasonic system, consisting of two waveguides, one of which is connected to a source of ultrasonic vibrations, while the other one represents the passive waveguide-reflector used to press a blank against it, as well as for purposes of vibroinsulation of the coupled vibratory system and reflection of elastic wave passed through the workpiece. Making use of the dynamic compliance operator of viscoelastic rod-shaped waveguide [19], it is possible to write now the equations for the longitudinal displacements of the strikers:

$$\begin{aligned} u_1 &= L_1(\omega)P_1(t) + L_1(\omega)\Phi(u_V, \dot{u}_V) - L_1(0)G, \\ u_2 &= -L_2(\omega)\Phi(u_V, \dot{u}_V). \end{aligned} \tag{1}$$

Here the values of displacements, u_1 and u_2, are measured starting from the end face positions in the waveguides unloaded; in other words, it is assumed that $u_1 = 0$ and $u_2 = 0$ for the waveguides unstrained. $u_V = u_1 - u_2$ is the relative displacement of the strikers' tops. $L_n(\omega)$ is the operator of dynamic compliance of the nth waveguide ($n = 1, 2$) that specifies the relationship between the contacting end face displacement and the longitudinal driving force (see Appendix A). Following Ref. [19], the excitation force $P_1(t) = P\cos\omega t$, that is generated by ultrasonic transducer, is assumed to be applied to the contacting end face of the active waveguide. The function $\Phi(u_V, \dot{u}_V)$ describes the force of contact interaction of waveguides in-between via the workpiece.

The method of harmonic linearization [5,19] makes it possible to seek for a solution of Eqs. (1) in the single-mode form:

$$u_n = m_n + a_n\cos(\omega t - \varphi_n), \quad u_V = m_V + a_V\cos(\omega t - \varphi_V), \tag{2}$$

where m_n and m_V are the constant (time-independent) components of displacements, a_n and a_V are amplitudes, φ_n and φ_V are the phase shifts of absolute and relative vibrations of the waveguides' end faces.

The distance between the strikers' tops, or width of the gap between the upper and lower strikers, can be represented as (see Figs. 1c and 2a)

$$l = l_0 + u_V = l_0 + m_V + a_V\cos(\omega t - \varphi_V), \tag{3}$$

where l_0 is the distance at time instant t_1 when the strikers are brought into a contact with the workpiece. In the impact regime, the period of vibrations is divided into two stages, more specifically, the feed of workpiece

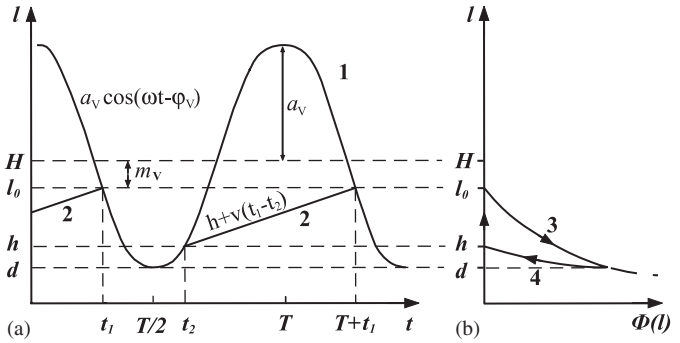

Fig. 2. (b) Time history of the gap width oscillation: curve 1 shows oscillation of relative distance between the strikers, curve 2 shows an increase in the work piece thickness due to continuous blank feed during the time interval of contact interruption (between two collisions); (b) deformation force dependence on the distance between the strikers: curve 3 shows an increase in force during the workpiece squeezing interval (when the strikers move one towards another), curve 4 shows a decrease in force during the interval of workpiece unloading (when strikers move in opposite directions). Arrows indicate the directions of deformation force variation during the working cycle.

into the site of deformation and the stage of deformation itself. The interval of plastic deformation lasts starting from the moment of contact, t_1, to the moment of contact break, t_2, i.e., at time instant when the relative vibration velocity of strikers moving in opposite directions becomes equal to that of the piece feed in the direction of vibrations: $a_V\omega \sin \omega t_2 = v$, where $v = 2V \tan a$. At time interval from t_2 to the next collision at time instant $T+t_1$ (at the point of intersection of curves 1 and 2, Fig. 2a), the upper and lower strikers perform back-and-forth motion in opposite directions. Curve 1 in Fig. 2a shows variation of distance between their flat tops. Curve 2 shows an increase in the workpiece thickness at the blank feed through the site of deformation in the workpiece feed interval, $[t_2, T+t_1]$. In order to make the model ideal, the following assumption is made:

- the upper and lower strikers are brought into contact with the piece at one and the same instant of time and the interruption of this contact for both strikers occurs simultaneously;
- within the entire working cycle, the velocity of feed, V, remains unchanged due to inertia of the blank rotation gear and rather short period of vibration.

The contact break thus takes place later as compared with the time instant of closest approach of strikers, $T/2$. Within the interval of gap widening from $T/2$ to t_2, the wedge-shaped surface of the blank pushes, due to blank feed, against the conical part of strikers. In the interval of the workpiece compression, $[t_1, T/2]$, one of the strikers moves oppositely to the other one and an increase of plastic deformation force can be approximated by inversely proportional dependence on the relative distance between the strikers (Fig. 2b, curve 3)

$$\Phi(l) = \frac{A}{l} + C. \tag{4}$$

The constant C can be easily found from the initial condition that $\Phi(l_0) = 0$; as a result, it gives $C = -A/l_0$. The phenomenological parameter A is specified by the geometry of deformation site, stress-strained state, and mechanical properties of the workpiece; it must be noted, however, that it is independent on the rate of deformation and ultrasound intensity [10].

In the interval of the workpiece unloading $[T/2, t_2]$, the strikers move in opposite directions and the inclined part of the workpiece alone is being deformed (by the conical surface of the strikers). Now, it is possible to approximate the contact unloading using as the base the linear law (Fig. 2b, curve 4):

$$\Phi(l) = K \cdot (l - h), \tag{5}$$

where $h = d + a_V(1 + \cos \omega t_2)$ is the distance between the strikers at time instant of contact interruption, t_2. The constant coefficient K in this formula can be found by proceeding from the initial condition for maximum value of the force $\Phi_{\max}(d) = A(1/d - 1/l_0)$ at the distance of the strikers' closest approach $l = d$. For each

working cycle, the force of resistance to plastic deformation or, that is just the same, the force of contact interaction between strikers can be thus described by the following piecewise smooth function [10]:

$$\Phi(l)=\begin{cases}0, & l\geqslant l_0, & 0\leqslant t\leqslant t_1,\\ A\left(l^{-1}-l_0^{-1}\right), & d\leqslant l\leqslant l_0, & t_1\leqslant t\leqslant \pi/\omega,\\ \frac{A}{dl_0}\cdot\frac{l_0-d}{h-d}(h-l), & d\leqslant l\leqslant h, & \pi/\omega\leqslant t\leqslant t_2,\\ 0, & l\geqslant h, & t_2\leqslant t\leqslant 2\pi/\omega,\end{cases} \tag{6}$$

where the moments of piecewise functions change are the following (see Fig. 2a):

$$t_1=\frac{\pi}{\omega}-\frac{1}{\omega}\arccos\frac{m_V}{a_V},\quad t_2=\frac{\pi}{\omega}+\frac{1}{\omega}\arcsin\frac{v}{a_V\omega}. \tag{7}$$

With the steady-state regime of ultrasonic micro-forging, the thickness, d, of the forged edge is constant. Both the distance, at which deformation starts to onset, l_0, and the distance at which it terminates, h, have the same value for every working cycle repeated. Since the striker rebounds from the workpiece, the upper vibration unit is lifted as a whole at a certain height H and remains practically immovable (since the total mass of the ultrasonic transducer and the pressing mechanism exceeds the effective mass of the stepped horn's front part). Obviously, the parameters d, l_0, h, H remain during every cycle invariable, if the thinning of the blade edge is compensated by feed of the workpiece in the stage of free motion of strikers (see Fig. 2a):

$$l_0-h=v[T-(t_2-t_1)]. \tag{8}$$

Without looking into the pattern of plastic yield in detail, it is seen that the herein-presented model makes it possible to describe the basic features of ultrasonic micro-forging: periodic interruption of contact (at vibro-impact regime), unlimited increase of strain resistance (shown by the extension of the dashed line 3, Fig. 2b) in the presence of the workpiece compression, weakening of contact when the strikers begin to move in opposite directions, and continuous drawing of blank edge through the vibrating gap.

The system of Eqs. (3), (7), and (8) must be completed with the relation (Fig. 2):

$$l_0+m_V=a_V+d\equiv H. \tag{9}$$

Making use of Eq. (9) and taking the condition $a_V\omega\gg v$ into account, it is possible to calculate the duration of deformation period (time of impact)

$$\tau=t_2-t_1\approx\frac{2\pi}{\omega}\sqrt{\frac{v}{\pi a_V\omega}}\left(1+\frac{1}{4}\sqrt{\frac{v}{\pi a_V\omega}}\right) \tag{10}$$

and the constant component of the relative displacement of the strikers:

$$m_V\approx a_V-\frac{2\pi v}{\omega}\left(1-\sqrt{\frac{v}{\pi a_V\omega}}\right). \tag{11}$$

3. Harmonic linearization

On substituting the variable l from Eq. (3) into Eq. (6) and carrying out the harmonic linearization in strict accordance with the formulas of Appendix B, it is possible to obtain the following relation for contact interaction force of strikers:

$$\Phi(l)=\Phi(u_V,\dot{u}_V)\cong f_0+(k+\mathrm{i}\omega\beta)a_V\mathrm{e}^{\mathrm{i}(\omega t-\varphi_V)}, \tag{12}$$

where the constant component of interaction force is as follows:

$$f_0 = \frac{A}{\pi}\left[\frac{1}{\sqrt{d(d+2a_V)}}\left(\frac{\pi}{2} - \operatorname{arctg}\sqrt{\frac{d(a_V+m_V)}{(d+2a_V)(a_V-m_V)}}\right) - \frac{1}{2(d+a_V-m_V)}\arccos\frac{m_V}{a_V}\right] + \frac{A}{\pi}\left[\frac{1}{2d}\left(\frac{a_V-m_V}{d+a_V-m_V}\right)\left(\frac{v}{a_V\omega}\right)\right]. \tag{13}$$

The harmonic coefficients of stiffness and damping are the following:

$$k = \frac{2A}{a_V\pi}\left[\frac{1}{2a_V}\arccos\frac{m_V}{a_V} - \frac{1}{a_V}\frac{d+a_V}{\sqrt{d(d+2a_V)}}\left(\frac{\pi}{2} - \operatorname{arctg}\sqrt{\frac{d(a_V+m_V)}{(d+2a_V)(a_V-m_V)}}\right)\right] + \frac{2A}{a_V\pi}\left[\frac{1}{2(d+a_V-m_V)}\left(\arccos\frac{m_V}{a_V} - \frac{v}{a_V\omega}\cdot\frac{a_V-m_V}{a_V}\right)\right], \tag{14}$$

$$\beta = -\frac{A}{\pi a_V\omega}\left[\frac{1}{a_V}\ln\left(1+\frac{a_V-m_V}{d}\right) - \frac{a_V-m_V}{a_V-m_V+d}\left(\frac{1}{a_V}+\frac{1}{2d}\left(\frac{v}{a_V\omega}\right)^2\right)\right].$$

If the permanent working load is balanced against the static pressure force, the upper vibration unit remains at rest, i.e., $f_0 = G$. For the sake of simplicity of the above-given expressions, it is then necessary to assume here that

$$\frac{a_V-m_V}{a_V} \ll 1 \text{ and } \frac{a_V-m_V}{d} \ll 1. \tag{15}$$

The physical meaning of this assumption is based on the supposition that the rigidity of contacting materials is sufficiently high; as is shown in Ref. [19], the exact equality $m_V = a_V$ within the limits of infinitely rigid (non-deformable) contact is met. The supposition is valid for our case of stainless steel cold working by use of strikers made of hard-alloy. Taking all this into account, jointly with the requirement that $a_V\omega \gg v$, it is possible to obtain from Eqs. (13–15) the below-given expressions:

$$d = \frac{\pi v}{\omega}\left[\sqrt{1+\frac{4A\omega}{GV\pi}\sqrt{\frac{v}{\pi a_V\omega}}} - 1\right], \tag{16}$$

$$k = -\frac{2G}{a_V} + \frac{A}{a_V^2\pi}\sqrt{\frac{v}{a_V\omega}}\left(4\sqrt{\pi} - \sqrt{\frac{v}{a_V\omega}}\right), \tag{17}$$

$$\beta = -\frac{G}{2a_V\omega}\sqrt{\frac{v}{a_V\omega}}\left(4\sqrt{\pi} - 3\sqrt{\frac{v}{a_V\omega}}\right). \tag{18}$$

Substitution of the value $v = 0$ in Eqs. (10), (11), and (16)–(18) leads to the exact coincidence with the data of calculations [2,19] as the approximation of infinitely large rigidity of contact:

$$\tau = 0, \quad m_V = a_V, \quad d = 0, \quad k = -\frac{2G}{a_V}, \quad \beta = 0.$$

For this reason, the approximation of infinite contact rigidity is included into the herein-presented model as a special case that corresponds to direct collision of strikers without the workpiece. It should be noted that the phenomenological constant A can be determined from Eq. (16) by measuring the thickness of the blank forged, d, provided that the values of all other processing parameters entering Eq. (16) are known. According to Eq. (9), the thickness of the forged blade edge can be determined by measuring a difference of dynamic drift, H, and the relative vibration amplitude, a_V, i.e., merely by measuring the dynamic characteristics of the ultrasonic setup itself.

This fact is of great importance for immediate control of the blade sharpness, since the measurements of a narrow, thin, and uneven burr by any other method are hard to be realized.

4. Dynamic response under loading

Subtraction of Eqs. (1), one from another, gives the equation for strikers' relative motion:

$$u_V = L_1(\omega)P_1(t) + [L_1(\omega) + L_2(\omega)]\Phi(u_V, \dot{u}_V) - L_1(0)G. \tag{19}$$

On substituting Eqs. (2) and (12) into Eq. (19) and separating the time-independent and fundamental harmonic terms, one obtains:

$$m_V = [L_1(0) + L_2(0)]f_0 - L_1(0)G, \tag{20}$$

$$a_V = L_1(\omega)P\mathrm{e}^{\mathrm{i}\varphi_V} + a_V[L_1(\omega) + L_2(\omega)](k + \mathrm{i}\omega\beta). \tag{21}$$

Limiting transition for static compliance of unfastened upper vibrator $L_1(0) \to \infty$ in Eq. (20) leads to earlier proven equality $f_0 = G$. Applying it to Eq. (20) gives

$$m_V = L_2(0)G. \tag{22}$$

Eq. (21) must be considered as the equation in the unknown a_V, because the harmonic coefficients k and β depend only on the relative amplitude a_V (see Eqs. (17) and (18)). Equating real and imaginary parts in Eq. (21) yields two coupled equations

$$\frac{P}{a_V}\cos\varphi_V = (\mathrm{Re}\,L_1(\omega) - kT(\omega) - \omega\beta S(\omega))Q_1^{-1}(\omega) \equiv U_V(\omega, a_V), \tag{23}$$

$$\frac{P}{a_V}\sin\varphi_V = -(\mathrm{Im}\,L_1(\omega) - kS(\omega) + \omega\beta T(\omega))Q_1^{-1}(\omega) \equiv -V_V(\omega, a_V), \tag{24}$$

where $Q_1(\omega) = \mathrm{Re}^2 L_1(\omega) + \mathrm{Im}^2 L_1(\omega)$, $T(\omega) = \mathrm{Re}\,L_1(\omega)\mathrm{Re}\,(L_1(\omega) + L_2(\omega)) + \mathrm{Im}\,L_1(\omega)\mathrm{Im}\,(L_1(\omega) + L_2(\omega))$, $S(\omega) = \mathrm{Im}\,L_1(\omega)\mathrm{Re}\,L_2(\omega) - \mathrm{Im}\,L_2(\omega)\mathrm{Re}\,L_1(\omega)$. $U_V(\omega, a_V)$ and $V_V(\omega, a_V)$ are the real and imaginary components of effective dynamical stiffness $W(\omega) = U_V(\omega, a_V) + iV_V(\omega, a_V)$ of coupled vibration system under the load [19].

The solution of Eqs. (23) and (24) is reduced to the transcendental equations for amplitude and phase response of vibration system loaded:

$$a_V = \frac{P}{\sqrt{U_V^2(\omega, a_V) + V_V^2(\omega, a_V)}}, \tag{25}$$

$$\tan\varphi_V = -\frac{V_V(\omega, a_V)}{U_V(\omega, a_V)}. \tag{26}$$

Substitution of harmonic coefficients k and β from Eqs. (17) and (18) into the expression for dynamical stiffness components $U_V(\omega, a_V)$ and $V_V(\omega, a_V)$ (given by. Eqs. (23) and (24)) reduces Eq. (25) to the irrational algebraic equation in the unknown a_v:

$$a_V^3\left[a_V^2 Q_1(\omega) + a_V M(\omega) + N(\omega)\right] + a_V\sqrt{a_V}\left[a_V^2 X(\omega) + a_V Y(\omega) + Z(\omega)\right] + I(\omega) = 0. \tag{27}$$

The coefficients that depend on the variable ω are the following:

$$M(\omega) = 4G(T(\omega)\mathrm{Re}\,L_1(\omega) + S(\omega)\mathrm{Im}\,L_1(\omega)), \qquad N(\omega) = 4G^2 + \left(T^2(\omega) + S^2(\omega)\right) - P^2Q_1^2(\omega),$$

$$X(\omega) = -4G\sqrt{\frac{\pi v}{\omega}}\left(Q_1(\omega)\mathrm{Im}\,L_1(\omega) - Q_2(\omega)\mathrm{Re}\,L_2(\omega)\right), \qquad Z(\omega) = -16AG\sqrt{\frac{v}{\pi\omega}}\left(Q_1^2(\omega) + Q_2^2(\omega)\right),$$

$$Y(\omega) = -8A\sqrt{\frac{v}{\pi\omega}}\left(Q_1(\omega)\mathrm{Re}\,L_1(\omega) + Q_2(\omega)\mathrm{Im}\,L_2(\omega)\right), \qquad I(\omega) = \frac{16A^2v}{\pi\omega}\left(Q_1^2(\omega) + Q_2^2(\omega)\right).$$

Each root of Eq. (27) that is found for the value of ω chosen and fixed values of other parameters specifies a point of AFC of relative vibration of contacting strikers. Substitution of this root value a_V into Eq. (26)

specifies a point of PFC at the same frequency. Treating the excitation frequency ω as an independent variable to calculate the roots of Eq. (27), one can plot the frequency response curves point by point.

The dependence of resonance frequency on vibration amplitude (which is peculiar to the nonlinear systems) can be described by the equation for the backbone curve:

$$\operatorname{Re} L_1(\omega) + \left(\frac{2G}{a_V} - \frac{4A}{a_V^2}\sqrt{\frac{v}{\pi\omega a_V^2}}\right) Q(\omega)_1 + \left(\frac{2G\pi}{a_V}\sqrt{\frac{v}{\pi\omega a_V^2}}\right) Q_2(\omega) = 0. \tag{28}$$

This equation has been derived from the condition $U_V(\omega, a_V) = 0$, which provides the largest amplitude value in Eq. (25). By analogy with procedure of construction of the amplitude and phase response curves, the backbone curve can be traced as a set of the roots of Eq. (28) calculated for different values of independent variable ω. Examination of Eq. (28) shows that the backbone curve is a double-valued function of ω and has a negative slope (see Figs. 3–5).

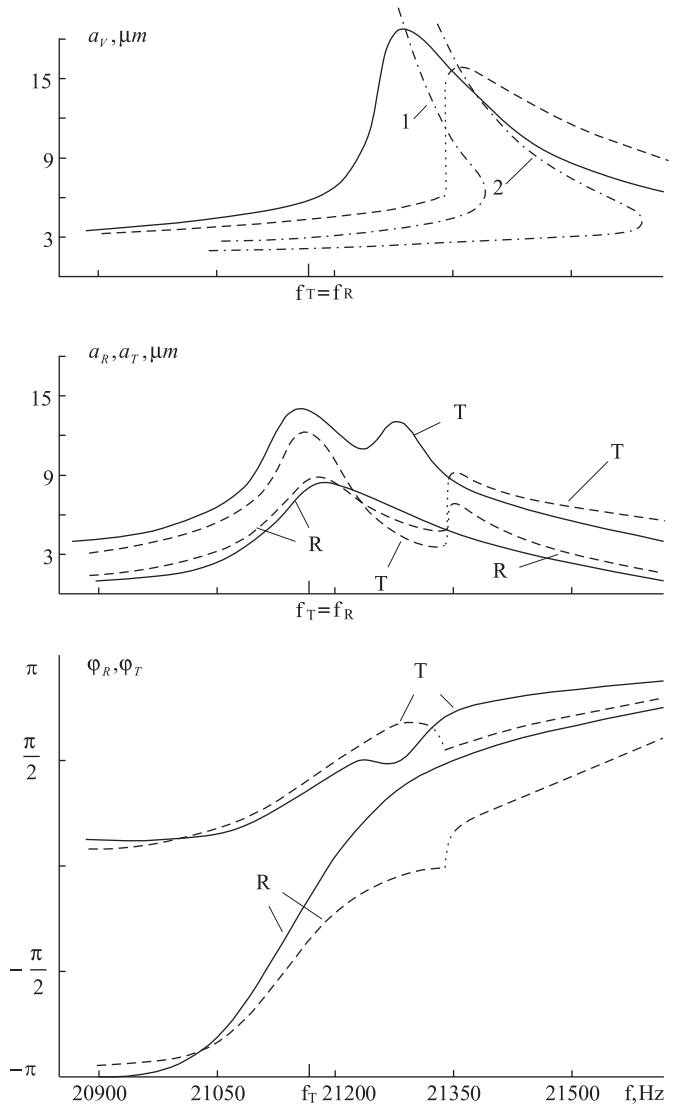

Fig. 3. Theoretical AFC and PFC of relative and absolute vibrations of strikers for $f_R = f_T$. The solid and dash lines correspond to static pressure force $G = 410$ N and $G = 600$ N, respectively; dot lines show unstable parts of characteristics (where the criterion Eq. (29) is violated); dash–dot lines show backbone curves of relative vibrations (described by Eq. (28)) for $G = 410$ N (curve 1) and $G = 600$ N (curve 2).

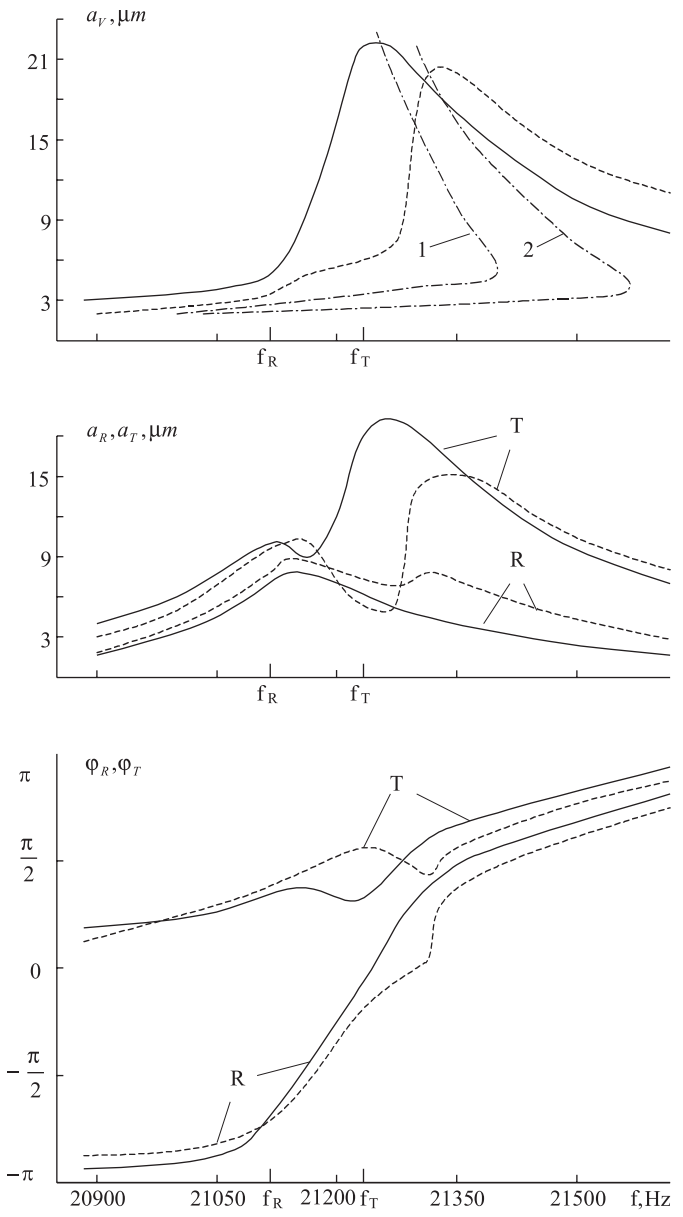

Fig. 4. The same as in Fig. 3 for $f_T > f_R$.

The peculiarities of this backbone curve give rise to an oscillation instability, so each root of Eq. (27) has been verified by use of stability criterion [19]:

$$U_V(\omega, a_V)\left(U_V(\omega, a_V) + a_V \frac{\mathrm{d}U_V(\omega, a_V)}{\mathrm{d}a_V}\right) + V_V(\omega, a_V)\left(V_V(\omega, a_V) + a_V \frac{\mathrm{d}V_V(\omega, a_V)}{\mathrm{d}a_V}\right) \geqslant 0. \tag{29}$$

Determination of a sign in the function (29) calculated for each root value of Eq. (27) allows to separate the stable solutions from unstable ones. Dot lines draw the unstable branches of amplitude and phase characteristics in Figs. 3 and 5.

Let us calculate now the responses for each of the contacting strikers. The substitution of Eqs. (2) and (12) into Eqs. (1) and application of harmonic balance method makes it possible to obtain, for oscillatory

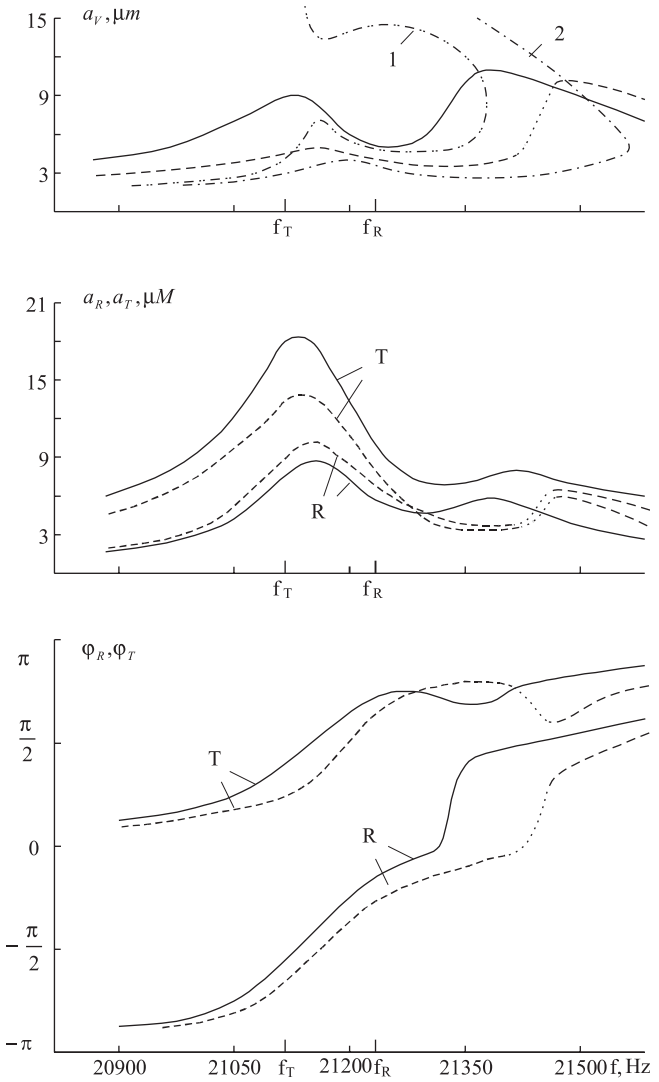

Fig. 5. The same as in Fig. 3 for $f_T < f_R$.

component of absolute motion of forced waveguide, the following equation

$$a_1 e^{-i\varphi_1} = L_1(\omega)P + L_1(\omega)[k + i\omega\beta]a_V e^{-i\varphi_V}, \tag{30}$$

while for the passive waveguide-reflector, it can be represented as

$$a_2 e^{-i\varphi_2} = L_2(\omega)[k + i\omega\beta]a_V e^{-i\varphi_V}. \tag{31}$$

Eliminating of unknown multiplier $a_V e^{-i\varphi_V}$ by use of Eq. (21) and separating the real and imaginary parts of Eqs. (30) and (31), it is possible to obtain:

$$\frac{P}{a_1}\cos\varphi_1 = \frac{\mathrm{Re}\, L_1(\omega)}{Q_1(\omega)} - \frac{k - \left(k^2 + \omega^2\beta^2\right)\mathrm{Re}\, L_2(\omega)}{B(\omega)} \equiv U_1(\omega, a_v), \tag{32}$$

$$\frac{P}{a_1}\sin\varphi_1 = -\frac{\mathrm{Im}\, L_1(\omega)}{Q_1(\omega)} - \frac{\omega\beta + \left(k^2 + \omega^2\beta^2\right)\mathrm{Im}\, L_2(\omega)}{B(\omega)} \equiv -V_1(\omega, a_v), \tag{33}$$

$$\frac{P}{a_2}\cos\varphi_2 = -\frac{\mathrm{Re}\,L_1(\omega)}{Q_1(\omega)} - \frac{\mathrm{Re}\,L_2(\omega)}{Q_2(\omega)} + \frac{kT(\omega) - \omega\beta S(\omega)}{\left(k^2+\omega^2\beta^2\right)Q_1(\omega)Q_2(\omega)} \equiv U_2(\omega, a_v), \tag{34}$$

$$\frac{P}{a_2}\sin\varphi_2 = \frac{\mathrm{Re}\,L_1(\omega)}{Q_1(\omega)} + \frac{\mathrm{Im}\,L_2(\omega)}{Q_2(\omega)} - \frac{\omega\beta T(\omega) + kS(\omega)}{\left(k^2+\omega^2\beta^2\right)Q_1(\omega)Q_2(\omega)} \equiv V_2(\omega, a_v), \tag{35}$$

where $B(\omega) = 1 - 2k\,\mathrm{Re}\,L_2(\omega) + 2\omega\beta\mathrm{Im}\,L_2(\omega) + \left(k^2+\omega^2\beta^2\right)Q_2(\omega)$. Solution of Eqs. (32)–(35) gives AFC and PFC for both of strikers attached to the working ends of the upper and lower waveguides:

$$a_n = \frac{P}{\sqrt{U_n^2(\omega, a_V) + \mathrm{i}\omega V_n^2(\omega, a_V)}}, \quad \tan\varphi_n = -\frac{V_n(\omega, a_V)}{U_n(\omega, a_V)}, \quad n = 1, 2. \tag{36}$$

Eqs. (36) specify the frequency responses of absolute vibration as the function of the relative amplitude a_V. Any point that belongs to the plot of absolute response can thus be easy calculated by substitution of the relative amplitude value (calculated as the root of Eq. (27) for the same frequency of excitation) into Eqs. (36). After substitution of the so-obtained relative amplitude a_V into Eqs. (9)–(11), it is possible to obtain the values of parameters describing the process of metal working such as, for instance, the blade sharpness d, impact duration τ, dynamic drift H, and the largest value of deformation force $\Phi_{\max}(d)$. The parameters that are of utmost significance for purposes of practical use in the ultrasonic technology of blade sharpening [7] are summarized in Table 1. The last column of this table presents the experimental values of the blade sharpness $d_{\exp}$ that have already been estimated in the course of direct optical measurements of real sizes of polished transverse microsections of blades.

The numerical calculations and construction of frequency response plots were carried out by making use of the parameters that are most suitable for the processing conditions given: $P = 1300\,\mathrm{N}$, $A = 4.3\times10^{-3}\,\mathrm{Nm}$, $v = 0.04\,\mathrm{m\,s^{-1}}$, $f_1 = 21\,230\,\mathrm{Hz}$, $f_2 = 21\,110\,\mathrm{Hz}$. The operator of dynamic compliance was calculated in Appendix A to be accurate to the second-order infinitesimal of the coefficient of ultrasonic absorption χ. The value of the absorption coefficient χ can be determined by comparing the 3 dB bandwidth of amplitude response in the waveguide unloaded (calculated by substitution of $G = 0$ and $v = 0$ into Eq. (36)) with experimental data of the resonance peak measured for the idling ultrasonic transducer (shown by the dotted lines in Figs. 5 and 6). By equating the theoretical and experimental values of this bandwidth, one can easily estimate the coefficient of absorption as $\chi = 0.048$. It is worthwhile to note that in the absence of any coupling, the 3 dB bandwidth of the bell-type amplitude peak is about 150 Hz and exceeds the natural frequency difference $|f_1 - f_2|$.

The construction of frequency response plots was carried out for the following ratios between the natural frequencies of the coupled waveguides, more specifically, for the ideal case of equality between the natural frequencies of both waveguides $f_T = f_R$ (Fig. 3), natural frequency of the active waveguide, f_T, (that is forced by the ultrasonic transducer), which is larger (Fig. 4) and smaller (Fig. 5) as compared with the natural frequency, f_R, of the passive waveguide-reflector. The symbols "T" and "R" denote here the natural frequencies and response curves that correspond to the waveguide connected to the transducer and the waveguide-reflector, respectively.

Table 1
Influence of static pressure force on resonance characteristics and deformation parameters

G (N)	a_V (μm) max[a]	f_V (Hz) max[b]	a_T (μm)	a_R (μm)	τ/T	$\Phi_{\max}(d)$(N)	H (μm)	d (μm)	$d_{\exp}$ (μm)
350	22.5	212 40	20.3	4.8	0.108	410	37.0	14.5	11–14
410	22.0	212 50	19.1	6.0	0.119	490	33.0	11.0	10–14
600	20.1	213 30	15.0	6.8	0.138	740	28.3	8.2	8–9
830	16.3	214 30	11.3	6.1	0.176	990	22.8	6.5	6–8

Each parameter within the table line is calculated with the use of the same frequency value, f_V, corresponding to the largest value of relative amplitude a_V. Calculations are made for the case when $f_T > f_R$.

[a]This column adduces the largest values of relative amplitude.

[b]This column adduces the excitation frequency values corresponded to the largest values of relative amplitude.

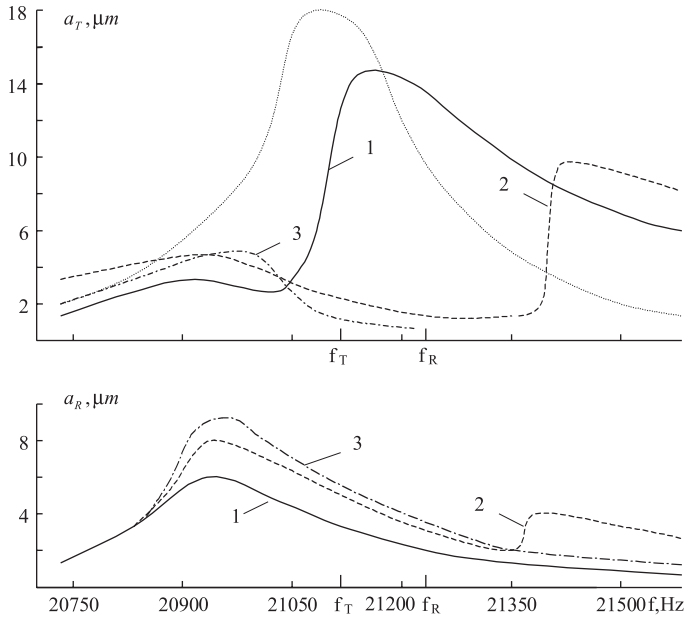

Fig. 6. Experimental AFC of waveguide that is forced by magnetostrictive transducer, a_T, and AFC of passive waveguide-reflector, a_R, in the course of ultrasonic micro-forging for $f_T < f_R$ and static pressure force $G = 410$ N, 600 N and 830 N (curves 1, 2 and 3, respectively). The dot line shows the AFC of the idling waveguide (without static load and worked material).

5. Comparison of experimental data and discussion of results

The theoretically obtained data of calculations were verified with the use of the experimental set up consisting of two impacting half-wavelength stepped horns that differ slightly in their natural frequencies. The waveguides were excited in turn through the magnetostrictive transducer of approximately 1 kW in power within the frequency range of 22 kHz. The upper and lower waveguides can be easily interchanged, so the inverse ratio between the natural frequencies of active and passive waveguides can be realized. A steel blade of 0.4 mm thick was fed through the vibrating gap between the strikers. The amplitudes and phases of vibration were measured with the use of the ring-type magnetic vibration detectors mounted on both waveguides.

The families of curves plotted for amplitude responses of these impacting waveguides (one of which being excited from the ultrasonic transducer) were measured for both ratios between the natural frequencies (confer Figs. 6 and 7).

Figs. 3–5 show the variations in the AFC and PFC (responses) with an increase in the static compression force, G, with values of all other technological parameters kept unchanged. The curve for the amplitude response of relative vibration envelops the backbone curve and follows its form. Distortions of the backbone curves show the influence of the load upon the resonance characteristics of strongly coupled vibro-impact system, especially in the case when $f_T < f_R$ (Fig. 5, curves 1 and 2). A pre-resonant branch of amplitude response curve becomes steeper as the compression force increases; the post-resonant branch becomes less steep.

When the excitation frequency lies below the resonance frequency, antiphase vibration of the waveguides takes place; it means that the strikers move in the same direction. Despite the large values of the strikers' absolute vibration amplitudes, the relative amplitude is small, especially in the case when $f_T < f_R$ (Fig. 5). At post-resonance frequencies, inphase vibration occurs with relative amplitude nearly equal to the sum of absolute amplitudes of the two strikers. At an instant of the strikers' collision, they move one towards another and strong impact action will provide thus the efficient processing.

On the other hand, the strong nonlinear (impact) interaction between these waveguides results in antiresonance damping of oscillation in the waveguide excited by transducer. The antiresonance frequency can be derived from the condition $U_1(\omega, a_V) \to \infty$ in Eq. (32). Neglecting the dissipative terms in this equation,

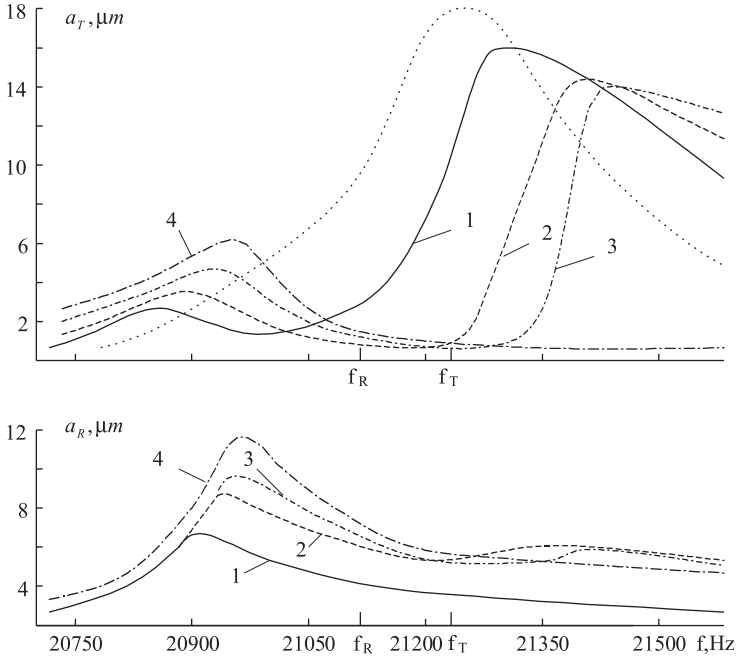

Fig. 7. The same as in Fig. 6 for $f_T > f_R$. Curves 4 are added for $G = 880$ N.

i.e., setting that $\beta = 0$ and $\chi = 0$, it is possible to obtain the approximate equation for estimation of antiresonance frequency value:

$$1 - k \operatorname{Re} L_2(\omega) = 0. \tag{37}$$

Substitution of the expression for the real part of the dynamic compliance operator that is derived in Appendix A into Eq. (37) gives

$$\xi_2 \cot \xi_2 + \frac{2G}{a_V} \cdot \frac{S_2}{E_2 F_2} = 0. \tag{38}$$

It is clear, that Eq. (38) is satisfied for negative values of $\cot \xi_2$ under $\xi_2 > \pi/2$, i.e. when an excitation frequency exceeds of natural frequency of passive waveguide $f > \gamma_2/4S_2 \equiv f_2$. By examining Eq. (38), it is seen that the antiresonance frequency lies always over the natural frequency of the waveguide-reflector, f_R, (irrespective of a natural frequency value of the waveguide excited, f_T). The antiresonanse drop changes the bell-type AFC of the waveguide excited into the double-hump form. The abrupt changes in AFC and PFC are indicative of the strong mutual influence of impacting waveguides. Distortions of the response curves become more noticeable with the strengthening of coupling that appears due to an increase in the force of static pressure. As a distinguishing feature from the linearly coupled oscillators [13], it is worth to note that both calculated resonance peaks in Figs. 3–5 are shifted just towards to the higher frequencies with respect to a given position of natural frequencies on the frequency axis.

The comparison of our results with the approximation of infinitely rigid contact [2,19] (that predicts a loss of oscillation stability, if the compression force exceeds the threshold $G = P/4$) shows certain distinctions that are due to the account of energy dissipation in the workpiece processed. So, for instance, a violation of criterion (29) takes place for the branches of amplitude response curves having the positive slope (Figs. 3 and 5, for $G = 600$ N); the threshold of stability is here considerably greater than $P/4$.

By and large, the data of our calculations are in a good agreement with those of the AFC measured (Figs. 6 and 7). Nonetheless, the spacing between two resonance peaks is somewhat greater than it is predicted by theory. The low-frequency peak lies below the lower natural frequency (of two) and it is typical for the linearly coupled oscillators [13]. Fig. 6 shows that the high-frequency peak of the excited waveguide is higher than the low-frequency peak (contrary to the theory, Fig. 5).

The above-noted discrepancies can be attributed to the assumptions adopted on the contact rigidity and expressed with use of the above-given inequalities (Eqs. (15)) and the requirement for impact interaction. At $a_V \to 0$, the harmonic coefficients k and β (Eqs. (17) and (18)) become hence infinite, while the derived here formulas describe correctly only the vibro-impact regime having the sufficiently large value of the relative amplitude a_V. At pre-resonance frequencies, the relative amplitude and velocity of strikers moving in the same direction have small values; as to the harmonic coefficients calculated by using formulas (17) and (18), they are overestimated. One can say that the real contact interaction of weakly impacting waveguides is more "soft" as compared with theoretical data from Eqs. (17) and (18) and that the behavior of the vibro-impact system is similar to that of oscillators with inseparable linear coupling [13].

In cases when the compression force exceeds a certain threshold, the vibro-impact regime terminates. The adjacent end faces of the waveguides experience the vibratory motion without any interruption of contact; within the entire period of vibration, the joint remains closed and the further processing becomes impossible (curve 3 in Fig. 6 and curve 4 in Fig. 7). At $f_T > f_R$ the threshold of compression force that corresponds to the contact closure and also the maximal attainable amplitude of relative vibration have the values that are significantly larger as compared with those at the inverse ratio of waveguides' natural frequencies. This fact can be explained by the relative location of resonance and antiresonance frequencies: the resonance peak of impact regime is being shifted towards the high-frequency region (in accordance with the backbone curve), while the antiresonance frequency of the excited waveguide lies always above the natural frequency of the waveguide-reflector (in accordance with Eq. (37)). In case when the waveguide connected with ultrasonic transducer has the natural frequency value lesser than that of the waveguide-reflector $(f_T < f_R)$, the frequency band of antiresonance damping overlaps the neighboring bandwidth of resonance peak of impact vibration. In case of inverse ratio $(f_T > f_R)$, the frequency bands corresponding to the antiresonance damping and resonance amplification of impact vibration are split by frequency f_T and spaced widely.

The relation $f_T > f_R$ ensures the stability of vibro-impact regime with the largest amplitude in the presence of the largest compression force; it has a certain advantage over the conventional equality of natural frequencies of both waveguides (confer the amplitude of relative vibration at the same value of compression force, Figs. 3 and 4). The optimal value of excess in the natural frequency of the excited waveguide depends on a design of ultrasonic set up used and the processing parameters, but it must not be larger than that of the resonance peak bandwidth.

6. Conclusions

1. The AFC and PFC of two nonlinearly coupled waveguides with somewhat unequal natural frequencies are calculated here by making use of the method for harmonic linearization. The contact interaction between the waveguides through the workpiece is approximated by a piecewise continuous function that makes it possible to describe the basic features of the vibro-impact regime.
2. The comparison of the model with two extreme cases, viz. (1) linear coupling and (2) infinitely rigid contact, reveals some similarities and distinctions that appear due to nonlinear and dissipative properties of the connecting link (workpiece).
3. The stable vibro-impact resonance needed to process the workpiece efficiently can be attained by meeting the rigorous requirement stating that the natural frequency of the ultrasonic transducer should exceed that of the waveguide-reflector.
4. The thickness of material forged can be directly controlled by measuring the dynamic response of the ultrasonic set up; the thickness of the forged workpiece is equal to the difference of dynamic shift of unfastened ultrasonic unit and the relative amplitude of the strikers vibration. This fact was verified in the course of metallographic measurements and has great practical importance.

Acknowledgments

The authors wish to thank Dr. Boguslavskii B.Z. at "MELITA-K" Ltd. for suggestion to use the ultrasonic forging in blade sharpening technology and for supplying with ultrasonic equipment.

Appendix A. Operator of dynamic compliance

The expression for the operator of dynamic compliance of waveguide was obtained in Ref. [19] by solving the longitudinal wave equation for the visco-elastic rod stressed by harmonic force at the working end and rigidly jammed at the mid plane.

Following Ref. [19], it is possible to write

$$L(\omega) = -\frac{\lambda\gamma^2}{EF\omega^2} \cdot \tanh(\lambda S), \tag{A.1}$$

where $\lambda = \mathrm{i}\omega/\sqrt{\gamma^2 + \mathrm{i}b\omega}$, E is the Young modulus, F and S are the cross-section area and the length of the rod, $b = \gamma^2\chi/2\pi\omega$ is the linearized coefficient of internal friction , γ is the sound velocity and χ is the sound absorption coefficient of the material the waveguide is made from. The second-order expansion in series of small value of absorption coefficient χ yields:

$$L_n(\omega) = \frac{S_n}{E_n F_n \xi_n} \cdot \frac{0.5\sin 2\xi_n - \xi_n(\chi_n/4\pi)^2 - \mathrm{i}(\chi_n/4\pi)(\xi_n + 0.5\sin 2\xi_n)}{\cos^2\xi_n + \left[(\chi_n/4\pi)\xi_n \sin\xi_n\right]^2}, \tag{A.2}$$

where the index $n = 1, 2$ denotes the upper and lower waveguides, respectively; $\xi_n = \omega S_n/\gamma_n$ is the dimensionless frequency for the nth waveguide. Static compliance of the waveguide is equal to longitudinal compliance of the rod with length S_n: $L(0) = S_n/E_nF_n$ at $\xi_n = \pi/2$, the first maximum of dynamic compliance gives the lowest value of natural frequency: $f_n = \gamma_n/4S_n$.

Appendix B. Coefficients of harmonic linearization

The coefficients of harmonic linearization of impact characteristic by Eq. (12) can be calculated according to the formulas [19]:

$$f_0 = \frac{1}{T}\int_0^T \Phi(l)\,\mathrm{d}t, \tag{B.1}$$

$$k = \frac{2}{Ta}\int_0^T \Phi(l)\cos\omega t\,\mathrm{d}t, \tag{B.2}$$

$$\beta = \frac{2}{Ta\omega}\int_0^T \Phi(l)\sin\omega t\,\mathrm{d}t, \tag{B.3}$$

where $T = 2\pi/\omega$ is the period of ultrasonic vibration.

Substitution of time-dependent variable l (Eq. (3)) into Eqs. (B.1)–(B.3) and division of the integration period into the same intervals in accordance with Eq. (6) allows to write Eqs. (13) and (14).

References

[1] V.P. Severdenko, V.V. Klubovich, A.V. Stepanenko, *Ultrasonic Rolling and Drawing of Metals*, Academic Press, New York, London, 1972.
[2] I.K. Vagapov, *Non-linear Effects in Ultrasonic Treatment*, Nauka i Technika, Minsk, 1987 (in Russian).
[3] J. Tsujino, Studies on ultrasonic plastic welding with two longitudinal vibration systems, *Japanese Journal of Applied Physics* 24 (1) (1985) 172–174.
[4] Z. Huang, M. Lucas, M.J. Adams, Influence of ultrasonics on upsetting of a model paste, *Ultrasonics* 40 (1–8) (2002) 43–48.
[5] V.K. Astashev, V.I. Babitsky, Ultrasonic cutting as a nonlinear (vibro-impact) process, *Ultrasonic* 36 (1) (1998) 89–96.
[6] M. Wiercigroch, J. Wojewoda, A.M. Krivtsov, Dynamics of ultrasonic percussive drilling of hard rocks, *Journal of Sound and Vibration* 280 (3–5) (2005) 739–757.
[7] I.K. Vagapov, A.S. Shinkarev, Plasticity and structure of metal forged by the use of ultrasound, *Metal Technology* 9 (1999) 8–10 (in Russian).
[8] S. Timoshenko, D.H. Young, W. Weaver Jr., *Vibration Problems in Engineering*, Wiley, New York, 1974.

[9] I.K. Vagapov, V.V. Klubovich, V.N. Sakevich, Excitation and stabilization of autoresonance impacting oscillations in ultrasonic technological systems, *Acuostica* 70 (1) (1990) 127–134.
[10] V.V. Klubovich, I.K. Vagapov, Model of plastic deformation of work-hardening material with ultrasound superimposition, *Doklady Akademii Nauk BSSR* 35 (4) (1991) 336–341 (in Russian).
[11] A. Cardoni, M. Lucas, Enhanced vibration performance of ultrasonic block horns, *Ultrasonics* 40 (1–8) (2002) 365–369.
[12] R.E. Mickens, O. Oyedeji, Dual periodic modes for two linearly coupled identical singular oscillators, *Journal of Sound and Vibration* 153 (3) (1992) 548–551.
[13] J. Söderkvist, An equivalent circuit description of two coupled vibrations, *Journal of the Acoustical Society of America* 90 (2) (1991) 693–699.
[14] L. Cveticanin, The motion of a two-mass system with non-linear connection, *Journal of Sound and Vibration* 252 (2) (2002) 361–369.
[15] H. Frosch, H. Büttner, Two coupled impact oscillators, *Zeitschrift für Physik B—Condensed Matter* 58 (4) (1985) 323–328.
[16] A. Cardoni, F.C.N. Lim, M. Lucas, M.P. Cartmell, Characterising modal interaction in an ultrasonic cutting system, *Forum Acusticum,* Seville, Spain, September 2002, paper ULT-02-003-IP.
[17] M. Lucas, Vibration sensitivity in the desing of ultrasonic forming dies, *Ultrasonics* 34 (1) (1996) 35–41.
[18] E. Pavloaskaia, M. Wiercigroch, Periodic solution finder for an impact oscillator with a drift, *Journal of Sound and Vibration* 267 (4) (2003) 893–911.
[19] V.I. Babitsky, *Theory of Vibro-Impact Systems*, Springer, New York, 1998.